Asymmetric Heterodinuclear $Fe^{III}M^{II}$ (M = Zn, Cu, Ni, Fe, Mn), $Co^{III}Fe^{II}$ and $Fe^{II}Co^{III}$ Species: Synthesis, Structure, Redox Behavior, and Magnetism

Sylvia Ross,[a] Thomas Weyhermüller,[a] Eckhard Bill,[a] Eberhard Bothe,[a] Ulrich Flörke,[b] Karl Wieghardt,[a] and Phalguni Chaudhuri*[a]

Keywords: Electrochemistry / Heterodinuclear complexes / Iron / Magnetic properties / Pyridine-2-aldoxime

Reactions of an LFe^{III} unit with an $M(PyA)_3^{n-}$ ion prepared in situ, where L represents 1,4,7-trimethyl-1,4,7-triazacyclononane and PyA^- is the monoanion of pyridin-2-aldoxime, yield heterodinuclear cations of the general formula $[LFe^{III}(PyA)_3M]^{2+}$, where M = Zn^{II} (**1**), Cu^{II} (**2**), Ni^{II} (**3**), low-spin Fe^{II} (**4**) and Mn^{II} (**5**). Additionally, we also prepared the diamagnetic species $[LCo^{III}(PyA)_3Fe^{II}]^{2+}$ (**6**). The $Fe^{III}Co^{II}$ species could not be isolated because a facile intramolecular electron transfer leads to complex **7**, $[LFe^{II}(PyA)_3Co^{III}]^{2+}$. Compounds **1**–**7** contain three oximato anions as bridging ligands and are isostructural in the sense that they all contain a terminal metal(III) ion in a distorted octahedral environment (e.g., FeN_3O_3) and a second six-coordinate metal ion M in a mostly trigonal-prismatic MN_6 geometry. Complexes **1**–**7** were characterized on the basis of elemental analyses, mass spectrometry, IR, UV/Vis, Mössbauer, and EPR spectroscopy, and variable-temperature (2–295 K) magnetic susceptibility measurements. The solid-state structures of **1**–**7** have also been determined by X-ray crystallography. The cyclic voltammograms of the complexes reveal both ligand-centered and metal-centered redox processes. Analysis of the susceptibility data indicates the presence of antiferromagnetic exchange interactions that decrease in the following order: $Fe^{III}Cu^{II}$ (**2**) > $Fe^{III}Ni^{II}$ (**3**) > $Fe^{III}Mn^{II}$ (**5**), as is expected. We have used X-band EPR spectroscopy of **3** ($Fe^{III}Ni^{II}$) at 2–6 K to establish the electronic ground state in great detail and to complement the magnetic susceptibility measurements.

Introduction

The field of research on heteropolynuclear complexes having different paramagnetic centers is still limited today by the small number of known and structurally fully characterized compounds and by the relative difficulty in synthesizing new compounds. Hence, the preparation of heteropolymetallic complexes has been a challenge for coordination chemists for many years.[1−3] Exchange-coupled heterometallic complexes are relevant to many different research areas, ranging from chemistry to solid-state physics and biology, because of their potential impact in material science, catalysis, and metallobiochemistry. Such exchange interactions in metalloproteins that involve more than one metal center have elicited the interest of bioinorganic chemists.[4−8]

We have adopted a synthetic strategy of using metal oximates as ligands for paramagnetic centers to increase the nuclearity and to synthesize heterometallic complexes. Thus, we have described a series of oximato-bridged (diatomic N,O-bridging) symmetrical and asymmetrical cores: M_AM_B,[9] $M_AM_BM_A$,[10] and $M_AM_BM_BM_A$[11] (M_A, M_B being two different metal ions). In addition, we have synthesized asymmetric heterotrinuclear complexes with cores $M_AM_BM_C$[12] and butterfly cores[13] $(M_A)_2(\mu\text{-}O)_2(M_B)_2$. Thus, we have synthesized linear heterotrinuclear complexes of general formula **A** and asymmetric dinuclear motifs $Cr^{III}\mu(O-N)_3M^{II}$ by using [tris(pyridinealdoximato)-metallate]$^-$ anions, $[M^{II}(PyA)_3]^-$, as ligands for the LCr^{III} unit, where L represents the tridentate cyclic amine 1,4,7-trimethyl-1,4,7-triazacyclononane.[9,10]

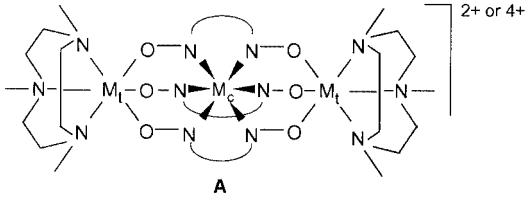

A

M_t = Fe^{III}, Mn^{III}, Mn^{IV}, Cr^{III}, Co^{III}

M_c = Zn^{II}, Cu^{II}, Ni^{II}, Fe^{II}, Mn^{II}

O−N N−O represents dioximate dianion

In this paper, we explore the effects of using Fe^{III} as the LM^{III} unit, i.e., $[LFe^{III}(PyA)_3M^{II}]^{2+}$ complex cations that are isostructural with the $[LCr^{III}(PyA)_3M^{II}]^{2+}$ centers. We

[a] Max-Planck-Institut für Bioanorganische Chemie, Stiftstraße 34−36, 45470 Mülheim an der Ruhr, Germany
E-mail: Chaudh@mpi-muelheim.mpg.de
[b] Universität − Paderborn, Warburgerstraße 100, 33098 Paderborn, Germany

  DOI: 10.1002/ejic.200300533

report the synthesis, magnetic, spectroscopic, and other physical properties of the following compounds, where M = Zn (**1**), Cu (**2**), Ni (**3**), Fe (**4**) and Mn (**5**).

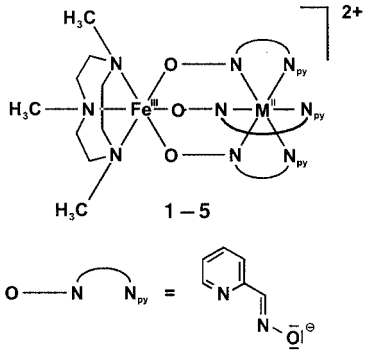

Additionally, we report the preparation and structural characterization of complexes $[LCo^{III}(PyA)_3Fe^{II}]^{2+}$ (**6**) and $[LFe^{II}(PyA)_3Co^{III}]^{2+}$ (**7**). Throughout this paper the compounds **1**–**7** are denoted by their metal centers only. Such isostructural series are not available for any other bridging ligands.

Results and Discussion

We utilized the high thermodynamic stability of the complex between Fe^{III} and the macrocycle 1,4,7-trimethyl-1,4,7-triazacyclononane together with the lability of the first transition series divalent metal ions to synthesize $Fe^{III}M^{II}$ dinuclear complexes. It is interesting to note that isolation of the intermediates $[M(PyA)_3]^-$ was not necessary during this synthetic route. Although no scrambling was observed, all attempts to strictly synthesize the cation $[LFe^{III}(PyA)_3Co^{II}]^{2+}$ under argon led to the isolation of **7**, $[LFe^{II}(PyA)_3Co^{III}]^{2+}$, as a result of facile intramolecular electron transfer. On the other hand, complex **6**, $[LCo^{III}(PyA)_3Fe^{II}]^{2+}$, was readily isolated starting from its respective materials. The colors of the heterometal dinuclear complexes **1**–**7** are light-to-deep-red/brown and they are air-stable in the solid state and also in solution for a few days, except for **7**.

Since the relevant bands in the IR spectra of comparable oxime-containing heteronuclear $Cr^{III}M^{II}$ complexes have been described earlier,[9] and the spectra of complexes **1**–**7** are also very similar, we refrain from discussing them in detail. The bands, together with their tentative assignments, are given in the Exp. Sect.

The electronic spectral results indicate that the complexes **1**–**7** are stable and retain their discrete dinuclear entities also in acetonitrile solution. Only complexes **3** and **7** exhibit lowest-energy spin-allowed d–d transitions at the Ni^{II} and Co^{III} centers, respectively. On the basis of their high extinction coefficients and transitions similar to those reported in the literature,[14] all bands below 350 nm (see Exp. Sect.) for complexes **1**–**7** are assigned to $\pi\rightarrow\pi^*$ transitions of the oxime ligand, whereas the bands above 400 nm, except at ca. 628, 729, and 891 nm for **3** and at 925 nm for **7**, are assigned to the MLCT and LMCT transitions indicating strong interactions of d orbitals with the conjugated π system of the oxime.[15] Judged on the basis of their low extinction coefficients, we tentatively ascribe the bands at ca. 628, 729, and 891 nm for **3** (Ni^{II}) and 925 nm for **7** (Co^{III}) to d–d transitions at the Ni^{II} and Co^{III} centers, respectively.

Electrospray-ionization mass spectrometry (ESI-MS) in the positive-ion mode proved to be a very useful analytical tool for characterizing complexes **1**–**7**. The major peaks are listed in the Exp. Sect. The ESI-MS results for **1**–**7** are very similar and show that, in most cases, there are only two peaks, which correspond to the monocation $[LFe(PyA)_3M(ClO_4)]^+$ and the dication $[LFe(PyA)_3M]^{2+}$. Interestingly, all the complexes show the doubly charged species $[LFe(PyA)_3M]^{2+}$ as the base peak (100%). There is practically no indication in the spectra for ligand fragmentation or cleavage of the dimer, which indicates the robustness of the clathrochelates,[16] i.e., multicyclic ligand systems that completely encapsulate a metal ion, derived from the pyridinealdoxime and the iron-containing capping agent. The data summarized in the Exp. Sect. show that mass spectrometry of the complexes demonstrates the nuclearity of all the complexes unambiguously and also provides a means for identification of the metal centers and the composition of the complexes. Complexes **1**–**7** are not fragile and can withstand the conditions of the ESI(pos)-MS ionization.[17]

Electrochemistry

Cyclic voltammograms (CV) of complexes **1**–**7** were measured at a glassy-carbon working electrode at ambient

Table 1. Cyclic voltammetric data in CH_3CN solutions: the reversible metal-centered oxidations and reductions of $[LM_A(PyA)_3M_B](ClO_4)_2$ **1**–**7**

Complex M_AM_B	$E_{1/2}^{ox}$ (M_A)	$E_{1/2}^{ox}$ (M_B)	$E_{1/2}^{red}$ (M_A)	$E_{1/2}^{red}$ (M_B)
1 $Fe^{III}Zn^{II}$		(+0.83)[a]	−0.80	
2 $Fe^{III}Cu^{II}$		+0.89	−0.62	
3 $Fe^{III}Ni^{II}$		+0.89	−0.72	
4 $Fe^{III}Fe^{II}$		+0.76	−0.62	
5 $Fe^{III}Mn^{II}$		+0.45, +0.73	−0.85, −1.07	
6 $Co^{III}Fe^{II}$		+0.53	−0.68	
7 $Fe^{II}Co^{III}$	+0.65	–	–	−0.63

[a] Ligand-centered oxidation; potentials in volts vs. Fc^+/Fc.

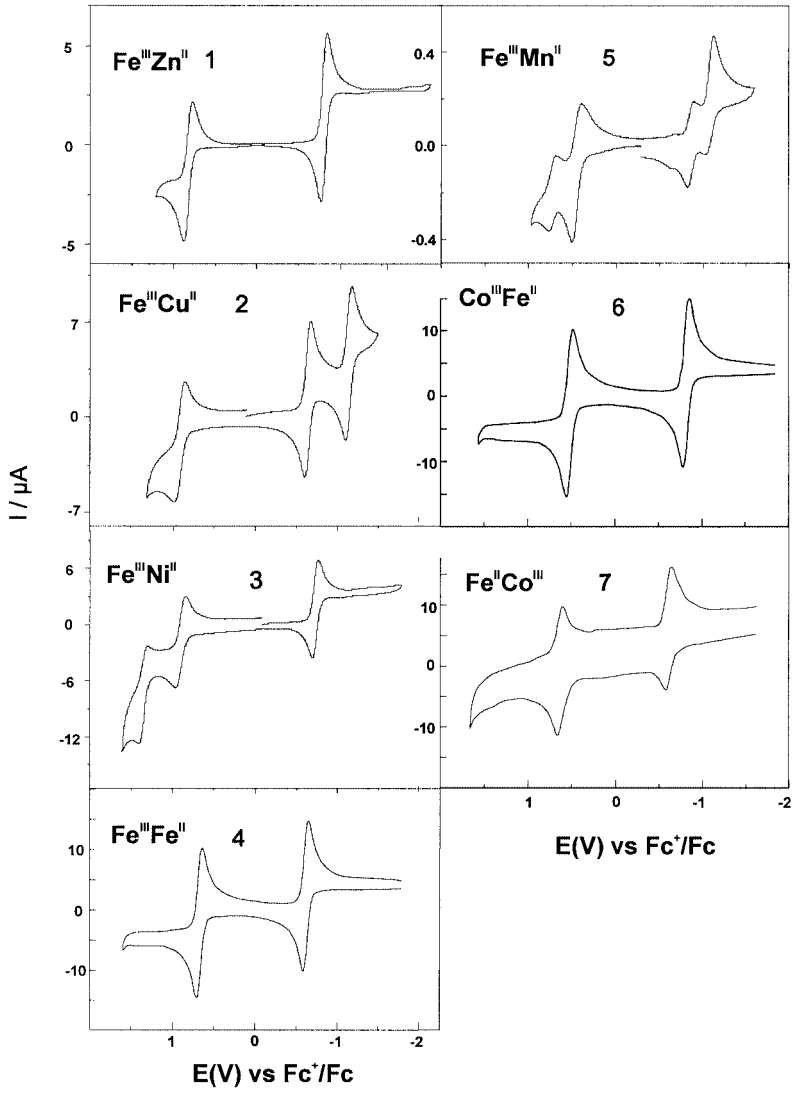

Figure 1. Cyclic voltammograms showing the reversible redox waves of complexes **1**−**7** in CH_3CN solutions containing 0.1 M nBu_4NPF_6; scan rates are 0.1 V/s, except for **5** where a scan rate of 1 V/s was used to achieve full reversibility of the first oxidative wave; working electrode: 2-mm glassy carbon or Pt disk; counter electrode: Pt; reference electrode: Ag/0.01 M $AgNO_3$ and referenced vs. Fc^+/Fc, added as an internal standard after each set of measurements

temperature in CH_3CN containing 0.1 M tetrabutylammonium hexafluorophosphate as the supporting electrolyte. The results are summarized in Table 1 and Figure 1. All redox potentials are referenced in V versus the ferrocenium/ferrocene couple (Fc^+/Fc) used as an internal standard, which is usually located at 0.09 V vs. Ag/0.01 M $AgNO_3$.

Each of the cyclic voltammograms of **1**−**7** (Figure 1) exhibits two reversible waves: one for an oxidation (in the range from +0.53 to +0.93 V) and one for a reduction (in the range from −0.62 to −0.85). The CV of **5** displays a particular feature: the oxidation and reduction are both split symmetrically into two components of unequal heights that are practically independent of the scan rate (0.3−3 V/s). The reason for this behavior is presently unknown. Apart from this exception, the heights of the peaks for oxidation and reduction of each complex are the same. Therefore, we conclude that they represent one-electron redox processes, since simultaneous, reversible two-electron oxidation *and* reduction of a mononuclear complex is not feasible. The two redox potentials for each complex, obtained from the voltammograms, are compiled in Table 1.

The reversible reductions observed for **1**−**7** in a relatively narrow potential range are assigned to the reduction of Fe^{III} (with **1**−**5**) or Co^{III} (with **6** and **7**) metal ions to their respective M^{II} forms. Complex **2** displays, in addition, a further reversible reduction wave at −1.14 V, which we assign to the Cu^{II}/Cu^{I} couple. At more negative potentials (ca. −2.0 V), further (irreversible) reductions occur for **3** and **5** (results not shown). These processes are assigned to ligand-centered reduction processes at the pyridin-2-aldoxime ligand in accordance with earlier observations[18] and results obtained with the analogous $Co^{III}Zn^{II}$ complex,[9] which exhibits *three* reversible reductions, with the one hav-

ing the lowest reduction potential (−1.83 V) being ligand-centered.

The reversible oxidations could be due either to oxidation of the M^{II} metal ions (M_B for **1**−**6** and M_A for **7**) to their M^{III} forms or to ligand oxidation. Clearly with complex **1**, which bears the "redox-inactive" metal ion $M_B = Zn^{II}$, the oxidation must be ligand-centered. The similarity of the redox potentials for all complexes **1**−**7**, irrespective of the nature of the M^{II} metal ions, could suggest that this phenomenon applies to all the complexes **1**−**7**. Nevertheless, we assign these reversible oxidations to the oxidations of the M^{II} metal ions M_B (for **2**−**6**) or M_A (for **7**) to their respective M^{III} forms, since ligand oxidation was observed only at potentials higher than +1.1 V for the analogous $Co^{III}M^{II}$, $Mn^{III}M^{II}$, and $Cr^{III}M^{II}$ complexes,[9] after metal-centered oxidation. Also, irreversible oxidation of this ligand in Ni^{II} complexes has been described in the literature,[18] again at potentials > 1.0 V. With **3** and **5**, we also observed such oxidation peaks at more positive potentials — at +1.42 and +1.36 V for **3** and **5**, respectively — and these processes are indeed assignable to oxidation of the pyridin-2-aldoxime ligand.

Mössbauer Isomer Shifts and Quadrupole Splittings

The Mössbauer spectra for **1**−**7** were measured at 80 K in zero field to determine the spin and oxidation states of the iron centers. The iron coordination environments are also different, i.e., $Fe^{III}N_3O_3$ for **1**−**5**, $Fe^{II}N_6$ for **4** and **6**, and $Fe^{II}N_3O_3$ for **7**. Each spectrum, except for that of **4**, was fitted with a single quadrupole split doublet, whose isomer shifts (δ_{Fe}) and quadrupole splitting (ΔE_Q) values are listed in Table 2. Mössbauer results, except for **4**, indicate a single quadrupole splitting in accordance with only one type of iron coordination sphere in the solid-state structure, namely the iron site coordinated to the cyclic amine, 1,4,7-trimethyl-1,4,7-triazacyclononane. An isomer shift of δ_{Fe} = 1.07 mm·s^{-1} and a quadrupole splitting of ΔE_Q = 3.66 mm·s^{-1} for **7** are consistent with those observed for high-spin iron(II) ions in octahedral and distorted octahedral environments.[19] The spectrum of **4** is a best fit to two equal-area doublets, which imply two iron sites having different coordination spheres, in agreement with the molecular structure of **4**, and, thus, they are assigned to the Fe^{III} and Fe^{II} ions. A comparison of the Mössbauer data for **1**−**5** with those for **6** and **7** indicates clearly the d^5 high-spin electron configuration for the iron centers coordinated to the cyclic amine. This assignment is also confirmed by the X-ray structures of **1**−**7**. The Mössbauer parameters of complexes **4** and **6** containing the $Fe^{II}N_6$ core are completely in agreement with those observed for low-spin iron(II) ions in octahedral and distorted octahedral environments. Summarily, the Mössbauer spectra[19] show unambiguously the high-spin nature of the Fe^{III} centers in complexes **1**−**5** and of the Fe^{II} center in complex **7**, containing FeN_3O_3 coordination environments, and the low-spin character of the Fe^{II} centers bonded to the nitrogen donor atoms of pyridin-2-aldoxime in complexes **4** and **6**.

Table 2. Mössbauer parameters at 80 K in zero-field

Complex	δ_{Fe} [mm·s^{-1}]	ΔE_Q [mm·s^{-1}]
1 $Fe^{III}Zn^{II}$	0.40	0.16
2 $Fe^{III}Cu^{II}$	0.45	0.01
3 $Fe^{III}Ni^{II}$	0.47	0.12
4 $Fe^{III}Fe^{II}$	0.41	0.39
	0.26	0.33
5 $Fe^{III}Mn^{II}$	0.46	0.43
6 $Co^{III}Fe^{II}$	0.30	0.40
7 $Fe^{II}Co^{III}$	1.07	3.66

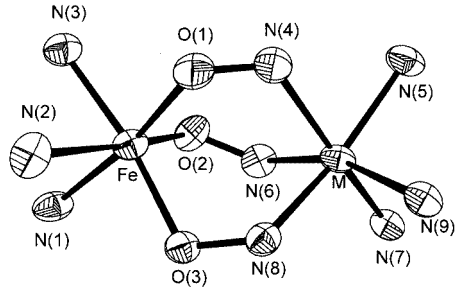

Figure 2. First coordination sphere of **3**, $Fe^{III}Ni^{II}$; the atom connectivities are identical for all complexes **1**−**7**

Table 3. Selected bond lengths [Å] for complexes $Fe^{III}Zn^{II}$ (**1**), $Fe^{III}Cu^{II}$ (**2**), $Fe^{III}Ni^{II}$ (**3**), $Fe^{III}Fe^{II}$ (**4**), and $Fe^{III}Mn^{II}$ (**5**)

	$Fe^{III}Zn^{II}$ (**1**)	$Fe^{III}Cu^{II}$ (**2**)	$Fe^{III}Ni^{II}$ (**3**)	$Fe^{III}Fe^{II}$ (**4**)	$Fe^{III}Mn^{II}$ (**5**)
Fe−N(1)	2.201(4)	2.187(3)	2.192(6)	2.202(6)	2.209(2)
Fe−N(2)	2.206(4)	2.201(3)	2.186(6)	2.174(8)	2.219(1)
Fe−N(3)	2.196(4)	2.186(3)	2.190(6)	2.195(8)	2.198(1)
Fe−O(1)	1.973(3)	1.950(2)	1.971(4)	1.963(5)	1.954(1)
Fe−O(2)	1.967(3)	1.993(2)	1.967(5)	1.970(7)	1.967(1)
Fe−O(3)	1.949(4)	1.967(2)	1.989(5)	1.976(7)	1.966(1)
$M^{II}-N(5)_{py}$	2.149(4)	2.293(3)	2.108(6)	1.977(7)	2.239(1)
$M^{II}-N(7)_{py}$	2.159(4)	2.114(3)	2.116(6)	1.990(8)	2.271(1)
$M^{II}-N(9)_{py}$	2.160(4)	2.023(3)	2.093(6)	2.001(8)	2.255(1)
$M^{II}-N(6)_{ox}$	2.155(4)	2.002(3)	2.052(6)	1.926(8)	2.243(1)
$M^{II}-N(8)_{ox}$	2.155(4)	2.129(3)	2.071(6)	1.907(8)	2.261(2)
$M^{II}-N(4)_{ox}$	2.205(4)	2.150(3)	2.063(6)	1.922(8)	2.242(1)

Molecular Structures of $[LFe^{III}(PyA)_3M^{II}](ClO_4)_2$ [M = Zn (1), Cu (2), Ni (3), Fe (4), Mn(5)]

The X-ray structures confirm that mixed-metal $Fe^{III}M^{II}$ complexes have indeed been formed with geometries in which two pseudooctahedral polyhedra are joined by three oximato N−O groups. The coordinated ligand L exhibits no unexpected features.[10,20] The N−O (average 1.355 ± 0.008 Å) and C=N_{ox} (average 1.287 ± 0.017 Å) bond lengths and C−N−O bond angle (average 117.8 ± 1.6°) of the bridging pyridinaldoximate ligand are very similar to those of other comparable structures.[9,21−24] Figure 2 illustrates the thermal ellipsoid plot of the $N_3Fe(O-N_{ox})_3M(N_{py})_3$ core for the $Fe^{III}Ni^{II}$ compound **3**. Table 3 lists bond lengths of the first coordination sphere of the $Fe^{III}M^{II}$ compounds **1**−**5**. As expected, the donor atoms for the metal ions of the cations in **1**−**5** are identical [FeN_3O_3 and $M^{II}(N_{ox})_3(N_{py})$], but the coordination geometry of the divalent metal centers are not. Perspective views of the cations are shown in Figure 3 for **1** and **2** and in Figure 4 for **3**, **4**, and **5**.

The iron coordination geometry is distorted octahedral with three nitrogen atoms, N(1), N(2), and N(3), from the facially coordinated tridentate macrocyclic amine L and three oxygen atoms, O(1), O(2), and O(3), from the bridging oximate group (Figure 2). The Fe−N (average 2.197 ±

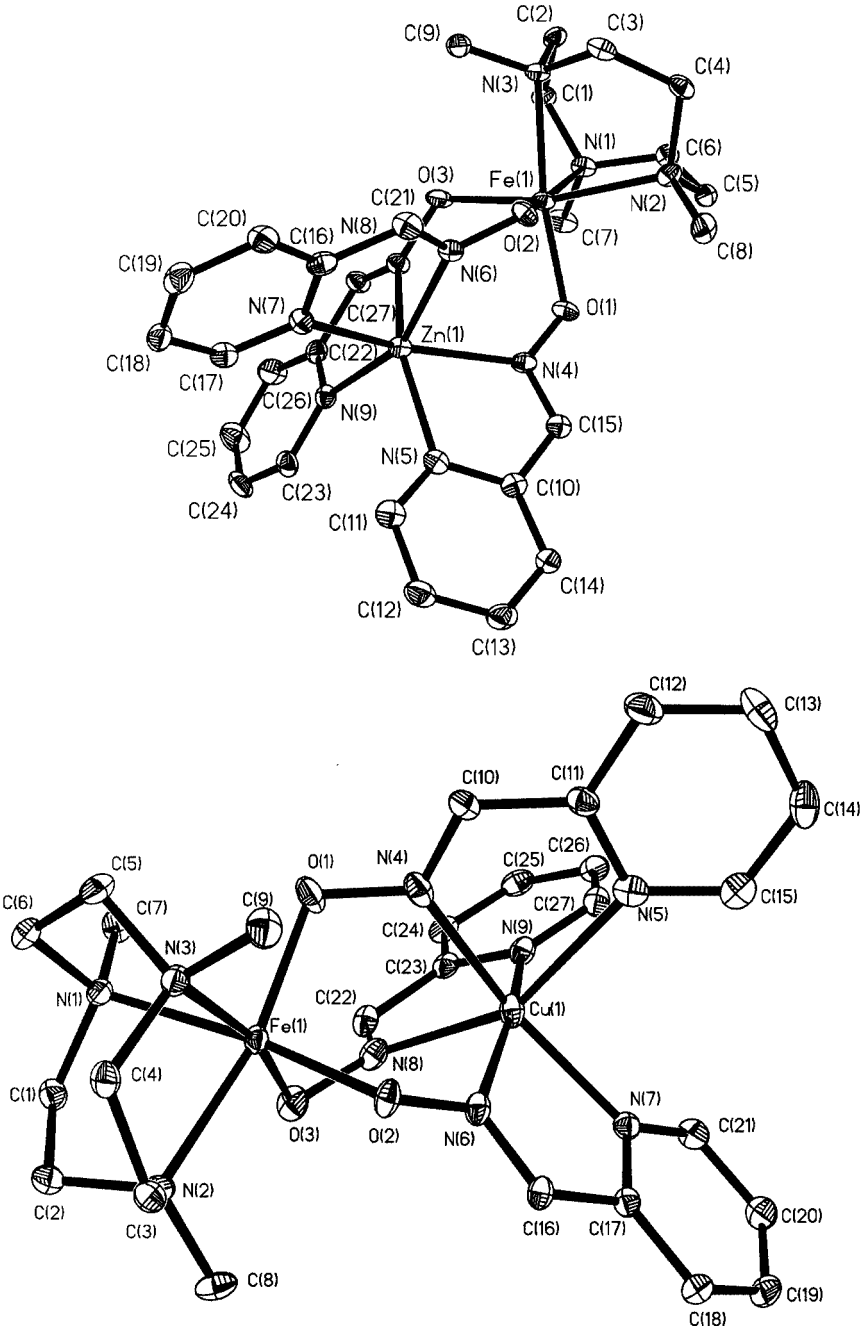

Figure 3. Molecular structures of the dications $Fe^{III}Zn^{II}$ in **1** (top) and $Fe^{III}Cu^{II}$ in **2** (bottom)

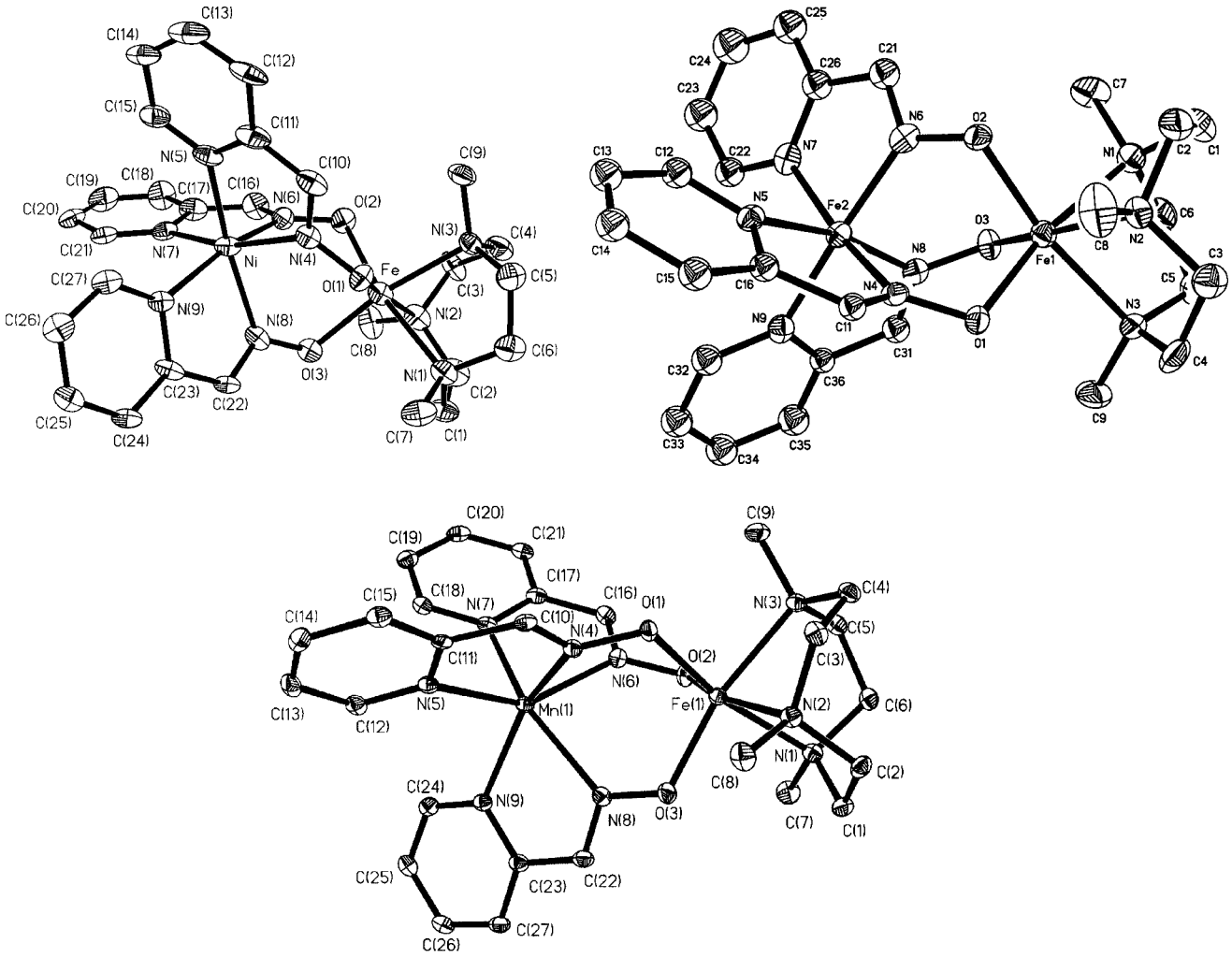

Figure 4. ORTEP diagrams of the complex cations showing the atom labeling schemes for $Fe^{III}Ni^{II}$ (**3**) (top, left), $Fe^{III}Fe^{II}$ (**4**) (top, right), and $Fe^{III}Mn^{II}$ (**5**) (bottom)

0.021 Å) and Fe−O (average 1.968 ± 0.020 Å) distances for complexes **1**−**5** correspond to those of known values[20,23] for Fe^{III} complexes with this macrocyclic amine, and are in agreement with a d^5 high-spin electronic configuration of the Fe^{III} centers, which is in complete agreement with the Mössbauer results. The largest deviation from the idealized 90° interbond angles is 12°, which occurs within the six-membered O−Fe−O chelate rings, the O−Fe−O angles ranging between 101.8(2) and 95.3(2)°, whereas the N−Fe−N angles fall between 78.95(5) and 81.1(3)°. The divalent second metal atom, which is separated from the ferric center at a distance 3.36−3.67 Å, does not affect the geometry of the ferric center. A similar observation has been made earlier for the analogous series of complexes featuring Cr^{III} ions.[9]

The crystal structure of complex **1** ($Fe^{III}Zn^{II}$) indicates the presence of two independent molecules crystallized with two molecules of solvent (methanol), which are hydrogen-bonded to two oxygen atoms of a perchlorate anion with O···O distances of 2.852 and 3.107 Å. We have found no substantial differences in the metrical parameters for the two independent molecules of **1**.

The second metal center, either Zn^{II}, Cu^{II}, Ni^{II}, Fe^{II}, or Mn^{II}, is also sixfold coordinated, yielding an MN_6 core. Coordination occurs facially through pyridine nitrogen atoms, $N_{py}(5)$, $N_{py}(7)$, and $N_{py}(9)$, and three azomethine nitrogen atoms, $N_{ox}(4)$, $N_{ox}(6)$, and $N_{ox}(8)$, from the pyridinaldoxime (PyA) ligand (Figure 2). The average M−N bond lengths fall within the ranges that are considered as normal covalent bonds for M^{II} centers with a high-spin configuration for Mn^{II} (d^5) (**5**), Ni^{II} (d^8) (**3**), and Cu^{II} (d^9) (**2**) and a d^6 low-spin electronic configuration for Fe^{II} (**4**). The low-spin electronic state of Fe^{II} in **4** has also been confirmed by the Mössbauer data.

The Cu−N distances and the angles N−Cu−N for **2** indicate that the resultant coordination sphere around the copper center in $Fe^{III}Cu^{II}$ is highly distorted. The smallest acute bite angle for *cis*-N−Cu−N occurs for the N(4)−Cu(1)−N(5) unit [73.3(1)°], where N(4) and N(5) atoms represent the oxime and pyridine nitrogen atoms, respectively, of the same pyridin-2-aldoximato ligand. On the other hand, the nitrogen atoms of the N(8)−Cu(1)−N(5) unit [154.3(1)°] belong to two different pyridinaldoximato ligands and the angle is the smallest

Table 4. Selected structural parameters for complexes **1**−**7**

Complex	$Fe^{III}\cdots M^{II}$ or $Co^{III}\cdots Fe^{II}$ or $Fe^{II}\cdots Co^{III}$ [Å]	Av. twist angle φ [°][a]	Dihedral angle θ [°][b]
1 $Fe^{III}Zn^{II}$	3.593(1)	30.3	34.9/39.4/35.4
2 $Fe^{III}Cu^{II}$	3.507(1)	35.2	40.0/34.4/43.9
3 $Fe^{III}Ni^{II}$	3.476(1)	39.2	43.5/37.4/37.5
4 $Fe^{III}Fe^{II}$	3.359(2)	46.3	39.6/43.7/43.9
5 $Fe^{III}Mn^{II}$	3.665(1)	22.3	28.7/36.2/31.3
6 $Co^{III}Fe^{II}$	3.389(1)	45.7	45.0/46.3/41.0
7 $Fe^{II}Co^{III}$	3.389(2)	50.4	50.8/51.1/49.9

[a] The trigonal twist angle φ is the angle between the triangular faces comprising N(4)N(6)N(8) and N(5)N(7)N(9) (Figure 2) and has been calculated as the mean of the Newman projection angles viewed along the centroids of focus. For an ideal trigonal prismatic arrangement, φ is 0° and 60° for an octahedron (or trigonal-antiprismatic arrangement). [b] That the core Fe(O−N)M is not linear is shown by the dihedral angles θ between the planes comprising Fe(O−N) and M(N−O) atoms.

among the *trans*-N−Cu−N angles, which indicates the severe deviation of the copper geometry from octahedral. No substantial differences in bond lengths and angles are found between the two crystallographically independent molecules of **2**.

For comparison, the important structural parameters are given in Table 4. It is clear from the data in Table 4 that the geometries of the metal ions Mn^{II} (**5**), Fe^{II} (**4**), Ni^{II} (**3**), Cu^{II} (**2**), and Zn^{II} (**1**) are distorted from octahedra toward trigonal prisms, as is evident from the twist angles; these distortions can be ascribed to both electronic (LFSE) and size effects, as has been discussed earlier.[9,10,25]

Molecular Structures of $[LCo^{III}(PyA)_3Fe^{II}](ClO_4)_2$ (6) and $[LFe^{II}(PyA)_3Co^{III}](PF_6)_2$ (7)

Figure 5 displays two perspective views of the cations in **6** and **7** and their atom labeling schemes. Selected bond lengths and angles are listed in Tables 5 and 6. The structural data concerning the ligand parts of the complex are in good agreement with the findings of previous studies dealing with compounds having the same ligands and do not warrant any additional comments. The X-ray structures confirm that the heterodinuclear complexes **6** and **7** have indeed been formed with a Co···Fe distance of 3.389 Å. The cobalt center in **6** and the iron center in **7** are distorted octahedra coordinated with three nitrogen atoms from the facially coordinated tridentate macrocyclic amine L and three oxygen atoms from the bridging oximate groups. The distances Co−N [average 2.011(3) Å] and Co−O [average 1.942(4) Å] in **6** and Fe−N [average 2.178(12) Å] and Fe−O [average 2.101(1) Å] in **7** correspond well with literature values for low-spin Co^{III} and high-spin Fe^{II} complexes, respectively.[20,26] The high-spin d^6 electronic configuration of the iron(II) center in **7** has also been confirmed by the Mössbauer and susceptibility measurements.

The second metal center, iron in **6** or cobalt in **7**, is also sixfold coordinated yielding an MN_6 core. Coordination occurs through three pyridine nitrogen atoms and three azomethine nitrogen atoms (Figure 5). The Fe−N (in **6**) and Co−N (in **7**) bond lengths (Tables 5 and 6) are consistent with a d^6 low-spin electron configuration for the metal centers, which was confirmed also by the magnetochemical measurements. Some pertinent structural parameters are listed in Table 4.

Magnetic Susceptibility and EPR Measurements

Magnetic susceptibility data for polycrystalline samples of the complexes were collected in the temperature range 2−290 K in an applied magnetic field of 1 T. We use the Heisenberg spin Hamiltonian in the form $H = -2J\cdot S_{Fe}\cdot S_M$ for an isotropic exchange coupling with $S_{Fe} = {}^5/_2$ and $S_M = 0$ for Zn^{II} (**1**), low-spin Fe^{II} (**4**), $S_M = {}^1/_2$ for Cu^{II} (**2**), $S_M = 1$ for Ni^{II} (**3**), and $S_M = {}^5/_2$ for Mn^{II} (**5**); for complex **7**, the spin states used are $S_{Fe} = {}^4/_2$ for a high-spin Fe^{II} ion and $S_{Co} = 0$ for a low-spin d^6 Co^{III} ion. The experimental data for **2**, **3**, and **5** for the effective magnetic moments (μ_{eff}) versus temperature (T) are displayed in Figure 6. The experimental magnetic data for the complexes (**1**−**5** and **7**) were simulated using a least-squares fitting program and the solid lines in Figure 6 represent the simulations for **2**, **3**, and **5**. Table 7 summarizes selected magnetic parameters with the observed spin ground states.

Complex **6** is diamagnetic indicating that both the cobalt and iron centers are in low-spin d^6 electron configurations, which is a finding that is also in full accord with the Mössbauer and structural parameters. Above $T \approx 25$ K, complexes **1** and **4**, which are magnetically mononuclear, exhibit essentially temperature-independent μ_{eff} values of 5.90 ± 0.02 and 5.80 ± 0.05 μ_B, respectively. Simulations of the experimental magnetic moment data yield g_{Fe} values of 2.0 for **1** and 1.96 for **4** with $S_{Fe} = {}^5/_2$ and $S_M = 0$. We note that the value of $g_{Fe} = 1.96$ for a high-spin ferric ion is comparatively low.

The magnetic moment μ_{eff}/molecule for **7**, Fe^{II}(h.s.)-Co^{III}(l.s.), of 5.30 μ_B ($\chi_M\cdot T = 3.517$ $cm^3\cdot K\cdot mol^{-1}$) at 290 K decreases monotonically with decreasing temperature until it reaches a value of 4.90 μ_B ($\chi_M\cdot T = 3.002$ $cm^3\cdot K\cdot mol^{-1}$) at 30 K and then starts to further decrease rapidly and reaches a value of 2.57 μ_B ($\chi_M\cdot T = 0.827$ $cm^3\cdot K\cdot mol^{-1}$) at 2 K. This temperature dependence is in agreement with a high-spin ferrous ion having an orbital T ground term. A least-squares fit results in a g_{Fe} value of 2.12.

The experimental magnetic moment for **2**, Fe^{III}(h.s.)Cu^{II}, is 5.55 μ_B ($\chi_M\cdot T = 3.853$ $cm^3\cdot K\cdot mol^{-1}$) at 290 K, which is

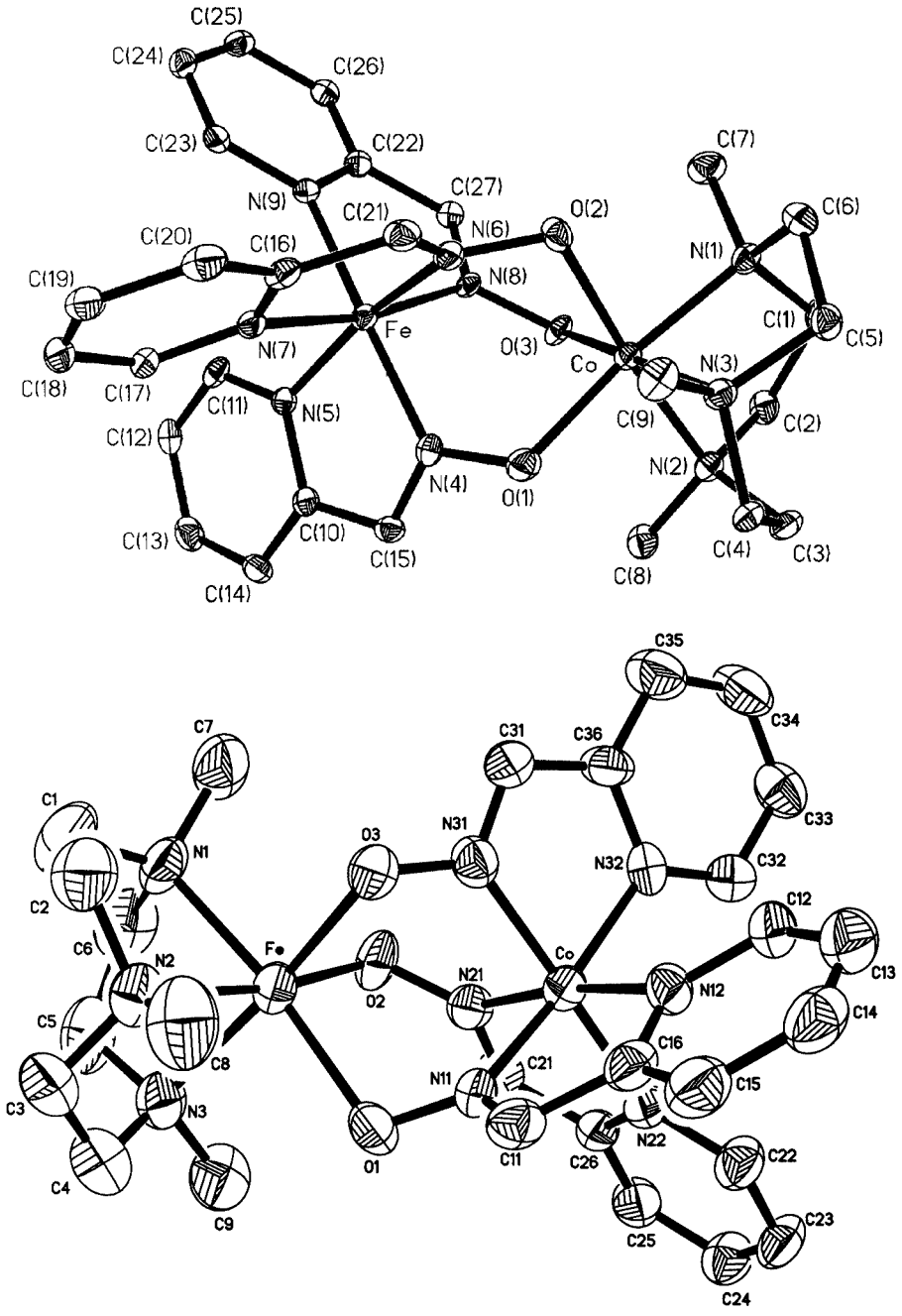

Figure 5. Perspective views of the cations in **6** ($Co^{III}Fe^{II}$) (top) and in **7** [Fe^{II}(h.s.)Co^{III}] (bottom)

significantly smaller than the theoretical value of μ_{eff} = 6.168 μ_B for two uncoupled spins of $S_{Fe} = {}^5/_2$ and $S_{Cu} = {}^1/_2$ with $g = 2.0$. Upon lowering the temperature, μ_{eff} decreases until a plateau is reached in the temperature range 80−40 K with a μ_{eff} value of ca. 4.88 μ_B ($\chi_M{\cdot}T$ = 2.974 $cm^3{\cdot}K{\cdot}mol^{-1}$), which is very close to the theoretical "spin-only" value of 4.90 μ_B for $S = 2$ expected as the ground state for an antiferromagnetically coupled $Fe^{III}Cu^{II}$ compound. Below 40 K, there is a decrease in μ_{eff} reaching a value of 3.27 μ_B ($\chi_M{\cdot}T$ = 1.341 $cm^3{\cdot}K{\cdot}mol^{-1}$) at 2 K. This deviation from the theoretical value is attributable to either zero-field splitting of the ground state $S_t = 2$ and/or intermolecular interactions. We have modeled this decrease with respect to the Weiss constant, θ. The least-squares fitting, shown as the solid line in Figure 6, of the experimental data leads to $J = -42.5\ cm^{-1}$, $g_{Fe} = 2.00$, $g_{Cu} = 2.05$, and θ = −0.4 K. The observed antiferromagnetic coupling ($J = -42.5\ cm^{-1}$) agrees well with the comparable exchange coupling constants reported earlier.[27]

The magnetic behavior of **3**, $Fe^{III}Ni^{II}$, is characteristic of an antiferromagnetically coupled dinuclear complex. At 290 K, the μ_{eff} value of 5.46 μ_B ($\chi_M{\cdot}T$ = 3.729 $cm^3{\cdot}K{\cdot}mol^{-1}$) decreases monotonically with decreasing temperature until it reaches a value of 3.53 μ_B ($\chi_M{\cdot}T$ =

Table 5. Selected bond lengths [Å] and angles [°] for $[LCo^{III}(PyA)_3Fe^{II}](ClO_4)_2$ in **6**

Co−O(3)	1.939(3)	Co−O(2)	1.941(3)
Co−O(1)	1.947(3)	Co−N(2)	2.001(3)
Co−N(3)	2.001(3)	Co−N(1)	2.011(3)
Fe−N(4)	1.889(3)	Fe−N(8)	1.894(3)
Fe−N(6)	1.898(3)	Fe−N(9)	1.967(3)
Fe−N(7)	1.979(3)	Fe−N(5)	1.984(3)
O(1)−N(4)	1.352(4)	O(2)−N(6)	1.350(4)
O(3)−N(8)	1.355(4)		
O(3)−Co−O(2)	93.29(12)	O(3)−Co−O(1)	94.74(11)
O(2)−Co−O(1)	94.74(12)	O(3)−Co−N(2)	88.22(12)
O(2)−Co−N(2)	174.61(12)	O(1)−Co−N(2)	90.29(12)
O(3)−Co−N(3)	174.60(12)	O(2)−Co−N(3)	91.69(13)
O(1)−Co−N(3)	86.92(12)	N(2)−Co−N(3)	86.63(13)
O(3)−Co−N(1)	91.95(12)	O(2)−Co−N(1)	88.34(12)
O(1)−Co−N(1)	172.46(12)	N(2)−Co−N(1)	86.44(13)
N(3)−Co−N(1)	86.11(13)	N(4)−Fe−N(8)	89.44(13)
N(4)−Fe−N(6)	89.49(14)	N(8)−Fe−N(6)	89.56(13)
N(4)−Fe−N(9)	167.26(13)	N(8)−Fe−N(9)	81.16(13)
N(6)−Fe−N(9)	98.97(14)	N(4)−Fe−N(7)	97.88(13)
N(8)−Fe−N(7)	168.01(13)	N(6)−Fe−N(7)	81.06(14)
N(9)−Fe−N(7)	92.87(13)	N(4)−Fe−N(5)	80.90(14)
N(8)−Fe−N(5)	96.60(13)	N(6)−Fe−N(5)	168.50(13)
N(9)−Fe−N(5)	91.59(13)	N(7)−Fe−N(5)	93.93(13)

Table 6. Selected bond lengths [Å] and angles [°] for $[LFe^{II}(PyA)_3Co^{III}](PF_6)_2$ in **7**

Co−N(21)	1.901(9)	Co−N(31)	1.911(9)
Co−N(11)	1.912(8)	Co−N(32)	1.964(8)
Co−N(22)	1.972(8)	Co−N(12)	1.985(8)
Fe−O(1)	2.099(7)	Fe−O(3)	2.101(8)
Fe−O(2)	2.102(7)	Fe−N(1)	2.166(9)
Fe−N(2)	2.179(9)	Fe−N(3)	2.190(10)
O(1)−N(11)	1.328(10)	O(2)−N(21)	1.322(10)
O(3)−N(31)	1.315(10)		
N(21)−Co−N(31)	90.34(4)	N(21)−Co−N(11)	91.4(4)
N(31)−Co−N(11)	90.9(3)	N(21)−Co−N(32)	93.5(4)
N(31)−Co−N(32)	81.8(3)	N(11)−Co−N(32)	171.3(4)
N(21)−Co−N(22)	82.7(4)	N(31)−Co−N(22)	171.9(4)
N(11)−Co−N(22)	93.3(3)	N(32)−Co−N(22)	94.5(3)
N(21)−Co−N(12)	171.8(4)	N(31)−Co−N(12)	94.0(3)
N(11)−Co−N(12)	81.6(3)	N(32)−Co−N(12)	94.1(3)
N(22)−Co−N(12)	93.5(3)	O(1)−Fe−O(3)	91.3(3)
O(1)−Fe−O(2)	92.1(3)	O(3)−Fe−O(2)	90.8(3)
O(1)−Fe−N(1)	171.7(4)	O(3)−Fe−N(1)	97.0(3)
O(2)−Fe−N(1)	87.6(3)	O(1)−Fe−N(2)	98.2(3)
O(3)−Fe−N(2)	89.8(3)	O(2)−Fe−N(2)	169.7(3)
N(1)−Fe−N(2)	82.2(4)	O(1)−Fe−N(3)	89.6(3)
O(3)−Fe−N(3)	171.4(4)	O(2)−Fe−N(3)	97.8(4)
N(1)−Fe−N(3)	82.2(4)	N(2)−Fe−N(3)	81.6(4)

1.561 $cm^3 \cdot K \cdot mol^{-1}$) at 10 K. A plateau in $\mu_{eff}(T)$ observed at 10−50 K indicates the presence of an energetically isolated ground state with total spin $S_t = {}^3/_2$ (spin-only value $\mu_{eff} = 3.87\ \mu_B$) according to a dominating exchange interaction between Fe^{III} ($S_{Fe} = {}^5/_2$) and Ni^{II} ($S_{Ni} = 1$). Below 10 K, there is a further decrease in μ_{eff} beyond what is expected from usual saturation due to zero-field splitting of the ground-state quadruplet. Magnetic susceptibility data were analyzed on the basis of a spin-Hamiltonian description of the electronic ground state of the single ions and their exchange interaction according to Equation (1), where $\mathbf{S}_i$ ($i = 1, 2$) are the spins of the metal ions in the dimers, D_i, E/D_i, and g_i are the local axial and rhombic zero-field parameters and g values, respectively, and J represents the exchange coupling constant.

$$H = \Sigma\{D_i[S_{z,i}^2 - S_i(S_i + 1)/3 + (E/D_i)(S_{x,i}^2 - S_{y,i}^2)] + \mu_B\mathbf{B}\cdot g_i\cdot\mathbf{S}_i\} - 2J\, S_1\cdot S_2 \quad (1)$$

The temperature dependence of μ_{eff} was well simulated by Equation (1) with parameters $J_{FeNi} = -34\ cm^{-1}$, $g_{Fe} = 2.0$ (fixed), $g_{Ni} = 2.12$ (fixed), $D_{Fe} = -1.1\ cm^{-1}$, $D_{Ni} = 5\ cm^{-1}$ (fixed), and 5.8% paramagnetic impurity with $S = {}^1/_2$. In the corresponding fitting procedure, the axial zfs parameter for nickel D_{Ni} was fixed to the value obtained from an isostructural $Co^{III}Ni^{II}$ complex having diamagnetic Co^{III} (not shown)[9] and the sign of D_{Fe}, as well as the value for g_{Ni}, was fixed according to the constraints derived from the EPR data (see below).

Solutions of compound **3** in BuCN/toluene (75:25, 0.4 mM) show resolved X-band EPR spectra (Figure 7). The derivative lines at $g \approx 4$ and 2 are typical of $S_t = {}^3/_2$ with strong axial zero-field splitting ($D_t > h\nu$) and low rhombicity ($0 > E/D_t > 0.1$). The presence of a distinct sharp peak at $g \approx 6$, which increases at lower temperatures, indicates the $|m_s = \pm{}^3/_2 >$ Kramers doublet to be the ground

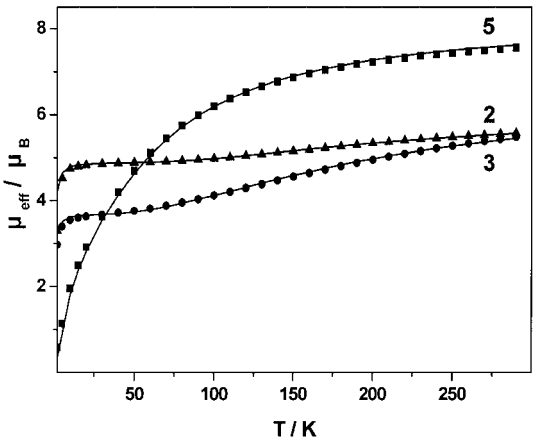

Figure 6. Plots of μ_{eff} vs. T for solid **2**, **3**, and **5**; the solid lines represent the best fit of the data to the Heisenberg−Dirac−van Vleck model (see text)

Table 7. Selected magnetic parameters for heterodinuclear complexes **1**−**7**

Complex	J [cm^{-1}]	g_{Fe}	g_M	Ground state (S_t)
1 $Fe^{III}Zn^{II}$	5.90 ± 0.02 μ_B	2.00	−	$S_t = {}^5/_2$
2 $Fe^{III}Cu^{II}$	−42.5	2.00	2.05	$S_t = 2$
3 $Fe^{III}Ni^{II}$ [a]	−34.0	2.00	2.12	$S_t = {}^3/_2$
4 $Fe^{III}Fe^{II}$(l.s.)	5.80 ± 0.05 μ_B	1.96	−	$S_t = {}^5/_2$
5 $Fe^{III}Mn^{II}$(h.s.)	−6.1	2.00	2.00	$S_t = 0$
6 Co^{III}(l.s.)Fe^{II}(l.s.)	diamagnetic			
7 Fe^{II}(h.s.)Co^{III}(l.s.)	5.1 ± 0.20 μ_B	2.12	−	$S_t = 2$

[a] $D_t = -1.8\ cm^{-1}$ (EPR), $D_t = -1.7\ cm^{-1}$ (susceptibility).

state, as a result of the negative zfs parameter D_t. The spectrum could be simulated reasonably well by using Equation (2) (see Exp. Sect.) for total spin $S_t = {}^3/_2$ with parameters $D_t = -1.8\ cm^{-1}$, $E/D_t = 0.078$, $g_t = (1.954, 1.954, 1.95)$, and isotropic g value $g_{t,iso} = 1.953$. The characteristic line shape of the powder spectrum was achieved by using a Gaussian distribution of the rhombicity parameter with a half-width $\sigma(E/D) = 0.078$.

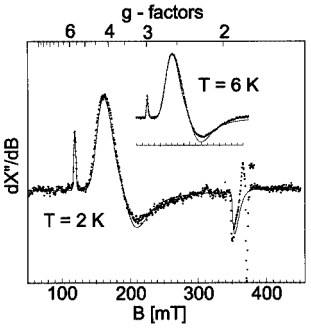

Figure 7. X-band EPR spectra of the $Fe^{III}Ni^{II}$ dimer **3** in BuCN/toluene solution recorded at 2 and 6 K (inset); experimental parameters: frequency = 9.4775 GHz, power = 2 μW (2 K)/20 μW (6 K), modulation = 1 mT/100 kHz; the solid lines are spin Hamiltonian simulations obtained using Equation (2) for total spin $S_t = {}^3/_2$ with parameters $D_t = -1.8\ cm^{-1}$, $E/D_t = 0.078$, $\sigma(E/D) = 0.078$, and $g_t = (1.954, 1.954, 1.95)$

The EPR parameter complements the interpretation of the magnetic data as given above. According to the spin projection properties, the ground-state parameters of complex **3** are related to the local single-ion values for iron and nickel by $D_t = (28/15)D_{Fe} + (1/15)D_{Ni}$ (neglecting dipolar contributions) and $g_t = 7/5\ g_{Fe} - 2/5\ g_{Ni}$. This finding indicates the dominant influence of the iron on the properties of the ground-state spin quadruplet. With the zfs value $D_{Fe} = -1.1\ cm^{-1}$ derived from the magnetic data (using fixed $D_{Ni} = 5\ cm^{-1}$), one obtains for the spin quadruplet $D_t = -1.7\ cm^{-1}$, which is strikingly close to the experimental value obtained from the EPR simulations ($-1.8\ cm^{-1}$). Hence, the complementary EPR and magnetic measurements determine the electronic properties of iron(III) and nickel(II) in **3** in great detail.

The μ_{eff} value for **5**, $Fe^{III}Mn^{II}$, decreases continuously from 7.64 μ_B ($\chi_M \cdot T = 7.299\ cm^3 \cdot K \cdot mol^{-1}$) at 290 K to 1.63 μ_B ($\chi_M \cdot T = 0.3304\ cm^3 \cdot K \cdot mol^{-1}$) at 2 K; this temperature dependence of μ_{eff} is a clear indication of an antiferromagnetic exchange coupling between two paramagnetic centers Fe^{III} ($S = {}^5/_2$) and Mn^{II} ($S = {}^5/_2$) with a resulting singlet ($S_t = 0$) ground state. Simulation of the experimental data (solid line in Figure 5) results in $J = -6.1\ cm^{-1}$, $g_{Fe} = g_{Mn} = 2.00$, and a paramagnetic impurity PI ($S = {}^5/_2$) = 0.3%.

Because a qualitative rationale for the trend of the antiferromagnetic exchange interactions between the spin carriers in the $Fe^{III}M^{II}$ pairs [M = Cu (**2**), Ni (**3**), and Mn (**5**)], on the basis of the established Goodenough−Kanamori rules[28] for superexchange as presented concisely by Ginsberg[29] and later by Kahn,[7] has been reported earlier,[3] we refrain from discussing it again in detail. Qualitatively, it can be said that the strength of exchange interactions increases upon decreasing the number of unpaired electrons, i.e., $Fe^{III}Mn^{II}$ (**5**) < $Fe^{III}Ni^{II}$ (**3**) < $Fe^{III}Cu^{II}$ (**2**), as the number of ferromagnetic paths operating in the interacting spin system decreases along the series shown above.

Several examples of structurally similar heterodimetallic complexes $Fe^{III}M^{II}$ (M = Zn, Cu, Ni, Co, or Mn) containing (μ-OR)bis(μ-carboxylato)-bridging ligands have been described in the literature[30−34] as models for dinuclear metal centers in proteins. Although the present exchange-coupled complexes **2**, **3**, and **5** having diatomic (−N−O) oximato bridges differ from the reported complexes,[30−34] it would be appropriate here to make a comparison of the efficacy of different bridging ligands with regard to the nature and magnitude of exchange couplings in the $Fe^{III}M^{II}$ pairs. The doubly or triply bridged $Fe^{III}M^{II}$ complexes exhibit exchange coupling varying from weakly ferromagnetic ($+4.2\ cm^{-1}$) to moderately antiferromagnetic ($-25\ cm^{-1}$). The bridging angle Fe−O(R)−M has been invoked[31] to rationalize this wide variation. In contrast, the tris(oximato)-bridged complexes **2**, **3**, and **5** are antiferromagnetically coupled, irrespective of the nature of the divalent metal center,[3,23,35] and, for comparable metal centers, they exhibit stronger exchange coupling than those reported in the literature,[31−35] although the Fe···M distances are significantly longer (ca. 0.2 Å) for the present complexes, which indicates that the oximato bridge is a better spin-coupler than either phenoxo or alkoxo groups.

Conclusions

In summary, we have synthesized and structurally characterized triply oximato-bridged heterodimetallic $Fe^{III}M^{II}$ complexes by using tris(pyridinaldoximato)metalates as ligands. This study confirms the essentially σ nature of the exchange interaction and applicability of the Goodenough−Kanamori rules in general to predict the nature of exchange interactions for different heterometal compounds containing the ferric ion in high-spin state. The strength of the antiferromagnetic interaction decreases in the following order: $Fe^{III}Cu^{II} > Fe^{III}Ni^{II} > Fe^{III}Mn^{II}$, as is expected.

The $Fe^{III}Co^{II}$ species could not be isolated because of facile intramolecular electron transfer leading to complex **7** ($Fe^{II}Co^{III}$). This finding is also in agreement with the cyclic voltammetric data.

The observation of the doubly charged species $[LFe(PyA)_3M]^{2+}$ as the base peak in each ESI-MS (positive) for all the complexes studied allowed the unambiguous characterization of these heterodimetal complexes.

Experimental Section

Materials and Physical Measurements: Reagent- or analytical-grade materials were obtained from commercial suppliers and used without further purification, except those for electrochemical measurements. Elemental analyses (C, H, N) were performed by the Micro-

analytical Laboratory, Dornis & Kolbe, Mülheim, Germany. Quantitative determination of manganese, iron, and cobalt was performed spectrophotometrically as their dipicolinic acid complexes.[36] Copper and nickel were determined gravimetrically by using *N*-benzoyl-*N*-phenylhydroxylamine and dimethylglyoxime, respectively. The perchlorate anion was determined gravimetrically as tetraphenylarsonium perchlorate. Fourier transform IR spectra of the samples in KBr disks were recorded with a Perkin−Elmer 2000 FT-IR instrument. Electronic absorption spectra in solution were measured with a Perkin−Elmer Lambda 19 spectrophotometer. Magnetic susceptibilities of powdered samples were recorded with a SQUID magnetometer in the temperature range 2−295 K with an applied field of 1 T. Experimental susceptibility data were corrected for the underlying diamagnetism using Pascal's constants and for the TIP contributions. Cyclic voltammetric and coulometric measurements were performed using EG & G equipment (potentiostat/galvanostat model 273A). Mass spectra were recorded with either a Finnigan MAT 8200 (electron ionization, EIMS) or a MAT 95 (electrospray, ESI-MS) instrument. A Bruker DRX 400 instrument was used for NMR spectroscopy. The Mössbauer spectrometer worked in the conventional constant-acceleration mode with a ^{57}Co/Rh source. Isomer shifts are given relative to α-Fe at room temperature. X-band EPR spectra were recorded with a Bruker ELEXSYS E500 spectrometer equipped with a helium flow cryostat (Oxford Instruments ESR 910). The spectra were simulated on the basis of a spin Hamiltonian description of the spin ground state manifold of the dimer molecules according to Equation (2), where S_t is the manifold and D_t and E/D_t are the axial and rhombic zero-field parameters.

$$H_e = D[S_{t,z}^2 - S_t(S_t+1)/3 + (E/D)(S_{t,x}^2 - S_{t,y}^2)] + \mu_B \mathbf{B}\cdot g\cdot \mathbf{S}_t \qquad (2)$$

The simulation program was developed from the $S = {}^5/_2$ routines of Gaffney and Silverstone and specifically makes use of the calculation of transition fields based on a Newton−Raphson iterative method as described.[38]

Preparations

$LFeCl_3$: This complex was prepared as described previously.[37]

$[LFe^{III}(PyA)_3M^{II}](ClO_4)_2$ [M^{II} = Zn (1), Ni (3), Fe (4), Mn (5)]: As complexes **1** and **3**−**6** were prepared in very similar manners, only a representative method is described. An argon-scrubbed solution of *syn*-pyridin-2-aldoxime (0.36 g, 3 mmol) in methanol (75 mL) was stirred with $M(ClO_4)_2\cdot 6H_2O$ (1 mmol) and triethylamine (0.5 mL) under argon for 0.5 h. Solid $LFeCl_3$ (0.33 g, 1 mmol) was added to the resulting solution and the stirring was continued under argon for a further 1 h before the mixture was filtered to remove any solid particles. The volume of the filtrate was reduced by passing argon over the surface of the solution until crystals began to separate. The crystals were collected by filtration and washed with diethyl ether.

Complex 1, $Fe^{III}Zn^{II}$: Red-violet crystals. Yield 0.33 g (39%). $C_{27}H_{36}Cl_2FeN_9O_{11}Zn$ (854.8): calcd. C 37.94, H 4.25, N 14.75, Fe 6.53, ClO_4 23.16; found: C 39.1, H 4.4, N 15.1, Fe 6.7, ClO_4 23.4. IR (KBr): $\tilde{\nu}$ = 1636 (CN), 1005 (NO), 1605, 1554, 1480, 1441 (pyridine) cm^{-1}. UV/Vis (CH_3CN): λ_{max} (ε) = 257 (25720), 303 (27300), 390 sh (ca. 4500) nm ($M^{-1}\cdot cm^{-1}$). ESI-MS: *m*/*z* (%) = 753, 654, 327 (100).

Complex 3, $Fe^{III}Ni^{II}$: Red-brown crystals. Yield 0.36 g (42%). $C_{27}H_{36}Cl_2FeN_9NiO_{11}$ (848.1): calcd. C 38.07, H 4.26, N 14.81, Fe 6.56, Ni 6.90, ClO_4 23.37; found C 38.0, H 4.2, N 14.7, Fe 6.7, Ni 6.8, ClO_4 23.5. IR (KBr): $\tilde{\nu}$ = 1636 (CN), 1007 (NO), 1605, 1584 1476, 1444 (pyridine) cm^{-1}. UV/Vis (CH_3CN): λ_{max} (ε) = 220 (33600), 255 (31910), 305 (29910), 513 sh (ca. 2100), 628 sh (ca. 102), 729 (40) nm ($M^{-1}\cdot cm^{-1}$). ESI-MS: *m*/*z* (%) = 747, 324 (100).

Complex 4, $Fe^{III}Fe^{II}$: Deep-red crystals. Yield 0.35 g (40%). $C_{27}H_{36}Cl_2Fe_2N_9O_{11}$ (845.2): calcd. C 38.37, H 4.29, N 14.91, Fe 13.21, ClO_4 23.43; found C 38.6, H 4.3, N 14.8, Fe 13.6, ClO_4 23.6. IR (KBr): $\tilde{\nu}$ = 1635 (CN), 1006 (NO), 1604, 1563 1467, 1435 (pyridine) cm^{-1}. UV/Vis (CH_3CN): λ_{max} (ε) = 202 (35660), 252 (23660), 294 (27550), 512 (8280) nm ($M^{-1}\cdot cm^{-1}$). ESI-MS: *m*/*z* (%) = 745, 323 (100).

Complex 5, $Fe^{III}Mn^{II}$: Deep-red crystals. Yield 0.34 g (40%). $C_{27}H_{36}Cl_2FeMnN_9O_{11}$ (844.3): calcd. C 38.41, H 4.30, N 14.93, Fe 6.61, Mn 6.51, ClO_4 23.56; found C 38.8, H 4.3, N 14.8, Fe 6.7, Mn 6.6, ClO_4 23.7. IR (KBr): $\tilde{\nu}$ = 1636 (CN), 1007 (NO), 1601, 1549 1466, 1437 (pyridine) cm^{-1}. UV/Vis (CH_3CN): λ_{max} (ε) = 257 (44670), 306 (43750), 393 (ca. 10880), 515 sh (ca. 2750) nm ($M^{-1}\cdot cm^{-1}$). ESI-MS: *m*/*z* (%) = 744, 322.5 (100).

$[LFe^{III}(PyA)_3Cu](ClO_4)_2$ (2): A sample of anhydrous copper(II) chloride (0.14 g, 1 mmol) and triethylamine (0.5 mL) was added with stirring under argon to a degassed solution of methanol (75 mL) containing *syn*-pyridin-2-aldoxime (0.36 g, 3 mmol). After 0.5 h, the stirred solution was charged with solid $LFeCl_3$ (0.33 g, 1 mmol) and the stirring was continued at ambient temperature for a further 1 h. After addition of $NaClO_4\cdot H_2O$ (0.75 g, 6 mmol), the volume of the solution was reduced by passing argon over the surface of the solution. The brown-red microcrystalline product was collected by filtration. X-ray-quality crystals were obtained from an acetonitrile solution. Yield 0.5 g (59%). $C_{27}H_{36}Cl_2CuFeN_9O_{11}$ (852.9): calcd. C 38.02, H 4.25, N 14.78, Fe 6.55, Cu 7.45, ClO_4 23.32; found C 38.1, H 4.4, N 14.6, Fe 6.6, Cu 7.6, ClO_4 23.5. IR (KBr): $\tilde{\nu}$ = 1635 (CN), 1006 (NO), 1606, 1583 1475, 1444 (pyridine) cm^{-1}. UV/Vis (CH_3CN): λ_{max} (ε) = 207 (31930), 240 (30390), 302 (26960), 525 sh (ca. 1640) nm ($M^{-1}\cdot cm^{-1}$). ESI-MS: *m*/*z* (%) = 752, 326.5 (100).

$[LCo^{III}(PyA)_3Fe^{II}](ClO_4)_2$ (6): Solid $Co(CH_3COO)_2\cdot 4H_2O$ (0.25 g, 1 mmol) was added to a degassed methanolic solution (25 mL) of 1,4,7-trimethyl-1,4,7-triazacyclononane (0.17 g, 1 mmol) under argon; the solution was stirred further for 1 h. A methanolic solution (50 mL) of (0.36 g, 3 mmol) of *syn*-pyridin-2-aldoxime and $Fe(ClO_4)_2\cdot 6H_2O$ (0.36 g, 1 mmol) was added to the cobalt-containing solution and then stirred at room temperature for 0.5 h. The precipitated black-violet microcrystalline substance was collected by filtration. X-ray-quality crystals were obtained by recrystallization from CH_3CN. Yield 0.42 g (50%). $C_{27}H_{36}Cl_2CoFeN_9O_{11}$ (848.3): calcd. C 38.23, H 4.28, N 14.86, Co 6.95, Fe 6.58, ClO_4 23.45; found C 38.2, H 4.1, N 14.5, Co 6.7, Fe 7.0, ClO_4 23.6. IR (KBr): $\tilde{\nu}$ = 1636 (CN), 1016 (NO), 1602, 1563 1467, 1434 (pyridine) cm^{-1}. UV/Vis (CH_3CN): λ_{max} (ε) = 209 (46500), 247 (42900), 270 sh (ca. 32400), 326 (23400), 527 (4100) nm ($M^{-1}\cdot cm^{-1}$). ESI-MS: *m*/*z* (%) = 748, 324.5 (100).

$[LFe^{II}(PyA)_3Co^{III}](ClO_4)_2$ (7): Methanol (25 mL) containing Et_3N (0.5 mL) was degassed at room temperature. Solid $Co(CH_3COO)_2\cdot 4H_2O$ (0.25 g, 1 mmol) and *syn*-pyridin-2-aldoxime (0.36 g, 3 mmol) were added to the methanol solution with continuous stirring over 0.5 h. $LFeCl_3$ (0.33 g, 1 mmol) was added to this clear solution and the stirring was continued for a further 1 h. Addition of $NaClO_4\cdot H_2O$ (0.5 g, 4 mmol) afforded a deep-red microcrystalline solid, which was collected by filtration and washed with diethyl ether. Yield 0.31 g (37%). $C_{27}H_{36}Cl_2CoFeN_9O_{11}$ (848.3): C 38.23, H 4.28, N 14.86, Fe 6.58, Co 6.95, ClO_4 23.45; found C 38.2,

Table 8. Crystallographic data for $[LFe(PyA)_3Zn](ClO_4)_2 \cdot CH_3OH$ (**1**), $[LFe(PyA)_3Cu](ClO_4)_2 \cdot CH_3CN$ (**2**), $[LFe(PyA)_3Ni](ClO_4)_2 \cdot CH_3OH$ (**3**), $[LFe(PyA)_3Fe](ClO_4)_2$ (**4**), and $[LFe(PyA)_3Mn](ClO_4)_2$ (**5**)

	$Fe^{III}Zn^{II}$ **1**	$Fe^{III}Cu^{II}$ **2**	$Fe^{III}Ni^{II}$ **3**	$Fe^{III}Fe^{II}$ **4**	$Fe^{III}Mn^{II}$ **5**
Empirical formula	$C_{28}H_{40}Cl_2FeN_9O_{12}Zn$	$C_{29}H_{39}Cl_2CuFeN_{10}O_{11}$	$C_{28}H_{40}Cl_2FeN_9NiO_{12}$	$C_{27}H_{36}Cl_2Fe_2N_9O_{11}$	$C_{27}H_{36}Cl_2FeMnN_9O_{11}$
Formula mass	886.81	893.99	880.15	845.2	844.34
Temperature [K]	100(2)	100(2)	100(2)	293(2)	100(2)
λ(Mo-K_α) [Å]	0.71073	0.71073	0.71073	0.71073	0.71073
Crystal system	monoclinic	monoclinic	monoclinic	triclinic	triclinic
Space group	$P2_1/c$	$P2_1/c$	$C2/c$	$P\bar{1}$	$P\bar{1}$
Unit cell dimensions [Å, °]	a = 20.050(4)	a = 19.7893(6)	a = 20.072(4) Å	a = 12.320(3) Å	a = 12.040(2) Å
	b = 24.346(4)	b = 24.6014(6)	b = 24.397(5)	b = 12.659(3)	b = 12.694(2)
	c = 15.079(3)	c = 15.1403(3)	c = 14.984(3)	c = 12.717(3)	c = 12.837(2)
				α = 100.02(1)	α = 110.62(2)
	β = 94.79(2)	β = 94.78(1)	β = 93.01(3)	β = 113.70(1)	β = 101.88(2)
				γ = 98.60(1)	γ = 101.25(2)
Volume [Å]^3; Z	7335(2), 8	7345.3(3), 8	7328(3), 8	1734.6(8), 2	1718.5(5), 2
Density (calcd.) [Mg/m^3]	1.606	1.617	1.596	1.618	1.632
Absorp. coeff. [mm^{-1}]	1.267	1.191	1.128	1.06	1.016
F(000)	3656	3680	3640	870	868
Crystal size [mm]	0.21 × 0.28 × 0.42	0.21 × 0.12 × 0.06	0.42 × 0.32 × 0.25	0.09 × 0.15 × 0.20	0.98 × 0.32 × 0.18
Diffractometer used	Siemens SMART	CAD 4	Siemens SMART	Siemens R3m/V	Siemens SMART
θ range for data collection [°]	1.59−25.51	2.07−30.0	1.67−23.24	1.5−27.5	1.78−34.02
Reflections collected	31266	157116	14222	8400	19767
Independent reflections	12364 (R_{int} = 0.0569)	21416 (R_{int} = 0.0964)	5218 (R_{int} = 0.1432)	8025 (R_{int} = 0.045)	11669 (R_{int} = 0.0171)
Data/restraints/parameters	12364/0/957	21387/0/975	5213/0/510	8025/0/373	11669/0/460
Goodness-of-fit on F^2	1.017	1.169	0.921	0.973	1.019
Final R indices [$I > 2\sigma(I)$]	R_1 = 0.0597,	R_1 = 0.0703,	R_1 = 0.0711,	R_1 = 0.099,	R_1 = 0.0364,
	wR_2 = 0.1481	wR_2 = 0.1143	wR_2 = 0.1433	wR_2 = 0.246	wR_2 = 0.0919
R indices (all data)	R_1 = 0.0945,	R_1 = 0.0992,	R_1 = 0.1315,	R_1 = 0.197,	R_1 = 0.0452,
	wR_2 = 0.1679	wR_2 = 0.1228	wR_2 = 0.1770	wR_2 = 0.332	wR_2 = 0.0978

Table 9. Crystallographic data for $[LCo^{III}(PyA)_3Fe^{II}](ClO_4)_2$ (**6**) and $[LFe^{II}(PyA)_3Co^{III}](PF_6)_2$ (**7**)

	$Co^{III}Fe^{II}$ **6**	$Fe^{II}Co^{III}$ **7**
Empirical formula	$C_{27}H_{36}Cl_2CoFeN_9O_{11}$	$C_{27}H_{36}CoF_{12}FeN_9O_3P_2$
Formula mass	848.33	939.37
Temperature [K]	100(2)	293(2)
λ(Mo-K_α) [Å]	0.71073	0.71073
Crystal system	triclinic	orthorhombic
Space group	$P\bar{1}$	$P2_12_12_1$
Unit cell dimensions [Å, °]	a = 12.020(3)	a = 12.283(3)
	b = 12.346(3)	b = 16.373(4)
	c = 12.693(3)	c = 18.387(5)
	α = 99.80(3)	
	β = 99.08(3)	
	γ = 113.43(3)	
Volume [Å^3], Z	1649.3(7), 2	3698(2), 4
Density (calcd.) [Mg/m^3]	1.708	1.687
Absorption coeff. [mm^{-1}]	1.179	1.032
F(000)	872	1904
Crystal size [mm]	0.32 × 0.20 × 0.38	0.30 × 0.17 × 0.14
Diffratometer used	Siemens SMART	Siemens R3m/V
θ range for data collection [°]	1.68−23.25	2.72−27.56
Reflections collected	6642	4734
Independent reflections	4665 (R_{int} = 0.0347)	4734 (R_{int} = 0.00)
Data/restraints/params	4664/0/463	4734/30/497
Goodness-of-fit on F^2	0.958	0.960
Final R indices [$I > 2\sigma(I)$]	R_1 = 0.0410,	R_1 = 0.055,
	wR_2 = 0.0993	wR_2 = 0.123
R indices (all data)	R_1 = 0.0542,	R_1 = 0.127,
	wR_2 = 0.1058	wR_2 = 0.169
Absolute structure parameter	−	0.07(4)

H 4.3, N 14.8, Fe 6.7, Co 7.0, ClO_4 23.6. IR (KBr): $\tilde{\nu}$ = 1620 (CN), 1010 (NO), 1602, 1560 1470, 1444 (pyridine) cm^{-1}. UV/Vis (CH_3CN): λ_{max} (ε) = 208 (37900), 243 (29370), 317 (16050), 516 (1710), 925 (20) nm ($M^{-1}\cdot cm^{-1}$). ESI-MS: *m*/*z* (%) = 748, 324.5 (100). X-ray-quality crystals of $[LFe(PyA)_3Co](PF_6)_2$ were obtained by addition of $NaPF_6$ as the anion source, instead of $NaClO_4$, from a methanolic solution.

CAUTION: Although we experienced no difficulties with the compounds isolated as their perchlorate salts, the unpredictable behavior of perchlorate salts necessitates extreme caution in their handling.

X-Ray Crystallographic Data Collection and Refinement of the Structures: The crystallographic data for **1**−**7** are summarized in Tables 8 and 9. Graphite-monochromated Mo-K_α radiation (λ = 0.71073 Å) was used throughout. X-ray diffraction data were collected at 293(2) K using a Siemens R3m/V diffractometer for **4** and **7**. Dark-red/brown to red crystals of **1**, **2**, **3**, **5**, and **6** were fixed with perfluoropolyether onto glass fibers and mounted on a Siemens SMART diffractometer (CAD 4 for **2**) equipped with a cryogenic nitrogen cold stream, and intensity data were collected at 100(2) K. Final cell constants were obtained from a least-squares fit of the setting angles of several strong reflections. Intensity data were corrected for Lorentz and polarization effects. An empirical absorption correction by ψ scans was applied for **4** and **7**. The data set for **2** was not corrected for absorption. The program SADABS (G. M. Sheldrick, Universität Göttingen, **1994**) was used for absorption corrections on data sets for **1**, **3**, **5**, and **6**. The Siemens ShelXTL software package (G. M. Sheldrick, Universität Göttingen) was used for solution, refinement, and artwork of the structures; the neutral atom scattering factors of the program were used. All structures were solved and refined by direct methods and difference Fourier techniques. Non-hydrogen atoms were refined anisotropically and hydrogen atoms were placed at calculated positions and refined as riding atoms with isotropic displacement parameters. For **4**, the aldoximic carbon atoms were refined isotropically. The methanol molecule and a perchlorate anion in **1** were found to be disordered and, therefore, a split-atom model was used. The two positions of the oxygen atom of the methanol molecule, O(70), were refined with two occupancies; O(70)/O(70X) = 0.8:0.2. CCDC-214728 (**1**), -214729 (**2**), -214730 (**3**), -214731 (**5**), -214732 (**6**), -212949 (**4**), and -212950 (**7**) contain the supplementary crystallographic data for this paper. These data can be obtained free of charge at www.ccdc.cam.ac.uk/conts/retrieving.html [or from the Cambridge Crystallographic Data Centre, 12 Union Road, Cambridge CB2 1EZ, UK; Fax: (internat.) + 44-1223-336-033; E-mail: deposit@ccdc.cam.ac.uk].

Acknowledgments

This work was initiated in Bochum. Our thanks are due to M. Winter (Bochum), H. Schucht, P. Höfer, A. Göbels, and B. Mienert for their skilful technical assistance. Support from the Max Planck Society and Fonds der Chemischen Industrie is gratefully acknowledged.

[1] O. Kahn, *Adv. Inorg. Chem.* **1995**, *43*, 179.
[2] K. S. Murray, *Adv. Inorg. Chem.* **1995**, *43*, 261.
[3] P. Chaudhuri, *Coord. Chem. Rev.* **2003**, *243*, 143.
[4] See, for example: R. H. Holm, E. I. Solomon (Guest Eds.), *Chem. Rev.* **1996**, *96 (7)*; A. L. Feig, S. J. Lippard, *Chem. Rev.* **1994**, *94*, 759; L. Que, A. E. True, *Progr. Inorg. Chem.* **1990**, *38*, 98; S. J. Lippard, J. M. Berg, *Principles of Bioinorganic Chemistry*, University Science Books, Mill Valley, CF, **1994**; W. Kaim, B. Schwederski, *Bioanorganische Chemie*, B. G. Teubner, Stuttgart, **1991**; *Bioinorganic Chemistry of Copper* (Eds.: K. D. Karlin, Z. Tyeklár), Chapman & Hall, New York, **1993**; *Mechanistic Bioinorganic Chemistry* (Eds.: H. Holden Thorp, V. L. Pecoraro), American Chemical Society, Washington, **1995**.
[5] *Magneto-Structural Correlations in Exchange Coupled Systems* (Eds.: R. D. Willett, D. Gatteschi, O. Kahn), Kluwer Academic Publishers, Dordrecht, **1985**.
[6] *Magnetic Molecular Materials* (Eds.: D. Gatteschi, O. Kahn, J. S. Miller, F. Palacio), Kluwer Academic Publishers, Dordrecht, **1991**.
[7] O. Kahn, *Molecular Magnetism*, VCH-Verlagsgesellschaft, Weinheim, **1993**.
[8] *Research Frontiers in Magnetochemistry* (Ed.: C. J. O'Connor), World Scientific, Singapore, **1993**.
[9] [9a] S. Ross, T. Weyhermüller, E. Bill, K. Wieghardt, P. Chaudhuri, *Inorg. Chem.* **2001**, *40*, 6656. [9b] S. Ross, Dissertation, Bochum, **1998**.
[10] D. Burdinski, F. Birkelbach, T. Weyhermüller, U. Flörke, H.-J. Haupt, M. Lengen, A. X. Trautwein, E. Bill, K. Wieghardt, P. Chaudhuri, *Inorg. Chem.* **1998**, *37*, 1009 and references cited therein.
[11] C. Krebs, M. Winter, T. Weyhermüller, E. Bill, K. Wieghardt, P. Chaudhuri, *J. Chem. Soc., Chem. Commun.* **1995**, 1913.
[12] C. N. Verani, T. Weyhermüller, E. Rentschler, E. Bill, P. Chaudhuri, *Chem. Commun.* **1998**, 2475; C. N. Verani, E. Rentschler, T. Weyhermüller, E. Bill, P. Chaudhuri, *J. Chem. Soc., Dalton Trans.* **2000**, 4263.
[13] P. Chaudhuri, E. Rentschler, F. Birkelbach, C. Krebs, E. Bill, T. Weyhermüller, U. Flörke, *Eur. J. Inorg. Chem.* **2003**, 541 and references cited therein.
[14] K. Burger, I. Ruff, F. Ruff, *J. Inorg. Nucl. Chem.* **1965**, *27*, 179.
[15] P. Krumholz, *Struct. Bonding* **1971**, *9*, 139.
[16] D. H. Busch, *Rec. Chem. Prog.* **1964**, *25*, 107.
[17] H. Budzikiewicz, *Mass Spectrometry*, Wiley-VCH, Weinheim, **1998**.
[18] M. Orama, H. Saarinen, J. Korvenranta, *Acta Chem. Scand.* **1989**, *43*, 407.
[19] [19a] P. Gütlich, R. Link, A. X. Trautwein, *Mössbauer Spectroscopy and Transition Metal Chemistry*, Springer-Verlag, Berlin, **1978**. [19b] P. Gütlich, in *Mössbauer Spectroscopy* (Ed.: U. Gonser), Springer-Verlag, Berlin, **1975**, chapter 2.
[20] P. Chaudhuri, K. Wieghardt, *Prog. Inorg. Chem.* **1987**, *35*, 329.
[21] [21a] R. Beckett, B. F. Hoskins, *J. Chem. Soc., Dalton Trans.* **1972**, *291*, 2527. [21b] M. Nasakkala, H. Saarinen, J. Korvenranta, M. Orama, *Acta Crystallogr., Sect. C* **1989**, *45*, 1511. [21c] G. A. Pearse, P. R. Raithby, J. Lewis, *Polyhedron* **1989**, *8*, 301. [21d] E. O. Schlemper, J. Stunkel, C. Patterson, *Acta Crystallogr., Sect. C* **1990**, *46*, 1226. [21e] K. W. Nordquest, D. W. Phelps, W. F. Little, D. J. Hodgson, *J. Am. Chem. Soc.* **1976**, *98*, 1104.
[22] P. Chaudhuri, M. Winter, U. Flörke, H.-J. Haupt, *Inorg. Chim. Acta* **1995**, *232*, 125.
[23] P. Chaudhuri, M. Winter, B. P. C. Della Vedova, P. Fleischhauer, W. Haase, U. Flörke, H.-J. Haupt, *Inorg. Chem.* **1991**, *30*, 4777.
[24] [24a] M. R. Churchill, A. H. Reis, Jr., *Inorg. Chem.* **1972**, *11*, 1811 [24b] M. R. Churchill, A. H. Reis, Jr., *Inorg. Chem.* **1972**, *11*, 2299. [24c] J. W. Faller, C. Blankenship, B. Whitmore, S. Sena, *Inorg. Chem.* **1985**, *24*, 4483. [24d] M. R. Churchill, A. H. Reis, Jr., *Inorg. Chem.* **1973**, *12*, 2280.
[25] [25a] R. A. D. Wentworth, *Coord. Chem. Rev.* **1972/73**, 9, 171. [25b]R. M. Kirchner, C. Meali, M. Bailey, N. Howe, L. P. Torre, L. J. Wilson, L. C. Andrews, N. J. Rose, E. C. Lingafelter, *Coord. Chem. Rev.* **1987**, *77*, 89. [25c] S. A. Kunow, K. J. Takeuchi, J. J. Grzybowski, A. J. Tircitano, V. L. Goedken, *Inorg. Chim. Acta* **1996**, *241*, 21.
[26] [26a] P. Chaudhuri, K. Wieghardt, B. Nuber, J. Weiss, *Angew. Chem. Int. Ed. Engl.* **1985**, *24*, 778. [26b] P. Chaudhuri, M. Win-

ter, H.-J. Küppers, K. Wieghardt, B. Nuber, J. Weiss, *Inorg. Chem.* **1987**, *26*, 3302.

[27] P. Chaudhuri, M. Winter, P. Fleischhauer, W. Haase, U. Flörke, H.-J. Haupt, *J. Chem. Soc., Chem. Commun.* **1993**, 566.

[28] [28a] J. B. Goodenough, *Magnetism and the Chemical Bond*, Wiley, New York, **1963**. [28b] J. B. Goodenough, *J. Phys. Chem. Solids* **1958**, *6*, 287. [28c] J. Kanamori, *J. Phys. Chem. Solids* **1959**, *10*, 87.

[29] [29a] A. P. Ginsberg, *Inorg. Chim. Acta Rev.* **1971**, *5*, 45. [29b] R. L. Martin, in *New Pathways in Inorganic Chemistry* (Eds.: Ebsworth, Maddock, Sharpe), Cambridge University Press, Cambridge, U. K., **1968**.

[30] S. K. Dutta, R. Werner, U. Flörke, S. Mohanta, K. K. Nanda, W. Haase, K. Nag, *Inorg. Chem.* **1996**, *35*, 2292.

[31] [31a] A. S. Borovik, L. Que, Jr., V. Papaefthymiou, E. Münck, L. F. Taylor, O. P. Anderson, *J. Am. Chem. Soc.* **1988**, *110*, 1986. [31b] T. R. Holman, K. A. Andersen, O. P. Anderson, M. P. Hendrich, C. Juarez-Garcia, E. Münck, L. Que, Jr., *Angew. Chem. Int. Ed. Engl.* **1990**, *29*, 921. [31c] T. R. Holman, C. Juarez-Garcia, M. P. Hendrich, L. Que, Jr., E. Münck, *J. Am. Chem. Soc.* **1990**, *112*, 7611. [31d] T. R. Holman, Z. Wang, M. P. Hendrich, L. Que, Jr., *Inorg. Chem.* **1995**, *34*, 134.

[32] R. M. Buchanan, M. S. Mashuta, J. F. Richardson, K. J. Oberhausen, R. J. Webb, M. A. Nanny, *Inorg. Chem.* **1990**, *29*, 1301.

[33] [33a] S. Albedyhl, M. T. Averbuch-Pouchot, C. Belle, B. Krebs, J. L. Pierre, E. Saint-Aman, S. Torelli, *Eur. J. Inorg. Chem.* **2001**, 1383. [33b] K. Schepers, B. Bremer, B. Krebs, G. Henkel, E. Althaus, B. Mosel, W. Müller-Warmuth, *Angew. Chem. Int. Ed. Engl.* **1990**, *29*, 531.

[34] [34a] L. Yin, P. Cheng, S.-P. Yan, X.-Q. Fu, J. Li, D.-Z. Liao, Z.-H. Jiang, *J. Chem. Soc., Dalton Trans.* **2001**, 1398. [34b] P. Karsten, A. Neves, A. J. Bartoluzzi, M. Lanznaster, V. Drago, *Inorg. Chem.* **2002**, *41*, 4624.

[35] [35a] P. Chaudhuri, M. Winter, P. Fleischhauer, W. Haase, U. Flörke, H.-J. Haupt, *J. Chem. Soc., Chem. Commun.* **1990**, 1728. [35b] M. Lengen, E. Bill, C. Butzlaff, A. X. Trautwein, M. Winter, P. Chaudhuri, *Hyperfine Interact.* **1994**, *94*, 1849.

[36] H. Hartkamp, *Z. Anal. Chem.* **1964**, *199*, 183.

[37] P. Chaudhuri, M. Winter, K. Wieghardt, S. Gehring, W. Haase, B. Nuber, J. Weiss, *Inorg. Chem.* **1988**, *27*, 1564.

[38] B. J. Gaffney, H. J. Silverstone, "Simulation of the EMR Spectra of High-Spin Iron in Proteins", in *Biological Magnetic Resonance* (Eds.: L. J. Berliner, J. Reuben), Plenum Press, New York, London, **1993**, vol. 13.

Received August 1, 2003

